Temperature-dependent Urbach tail measurements of lutetium aluminum garnet single crystals

Temperature-dependent Urbach tail measurements of lutetium aluminum garnet single crystals

M. Letz,[1] A. Gottwald,[2] M. Richter,[2] V. Liberman,[3] and L. Parthier[4]
[1]*Schott AG, Research and Development, Hattenbergstr. 10, D-55014 Mainz, Germany*
[2]*Physikalisch-Technische Bundesanstalt (PTB), Abbestr. 2-12, D-10587 Berlin, Germany*
[3]*Lincoln Laboratory, MIT, 244 Wood St., Lexington, Massachusetts 02420-9108, USA*
[4]*Schott Lithotec AG, Otto-Schott-Str. 13, D-07745 Jena, Germany*
(Received 10 November 2009; revised manuscript received 29 January 2010; published 14 April 2010)

Lutetium aluminum garnet (LuAG) is the most promising candidate for a high-index lens material for use in microlithographic imaging lenses. In the deep ultraviolet spectral range the transmission of high-purity LuAG was measured using monochromatized synchrotron radiation. In the vicinity of the band gap below 7.8 eV, a scaling behavior of the absorption as a function of photon energy was observed. Temperature-dependent measurements allowed us to distinguish different absorption mechanisms which differ by their ability to couple to phonon excitations. Interpreting the Urbach tails measured at different temperatures, it was shown that the temperature independent tail is due to defects in the lattice, whereas the temperature-dependent part originates from the short term localization of exciton modes coupling to lattice distortions. These results allowed us to extrapolate the maximum transmittance which can be obtained with LuAG crystals at the lithographic wavelength of 193.39 nm. Accurate determination of the maximum transmission limit is critical in deciding whether the material can meet industry's specification for 193-nm-based high-index lithography.

DOI: 10.1103/PhysRevB.81.155109 PACS number(s): 78.40.−q, 78.55.Hx, 78.90.+t

I. INTRODUCTION

According to the recent technology roadmap for semiconductors, high-end microlithographic semiconductor manufacturing nowadays (2009) is still performed with ArF excimer laser radiation at the wavelength of 193.39 nm, despite the written structures being significantly smaller than this wavelength. Several methods are used and tried to get beyond the classical diffraction limit in optical imaging, e.g., double exposure where neighboring patterns are illuminated with different masks (double patterning). A different attempt is immersion lithography: By the use of immersion fluids, the effective numerical aperture NA, the sinus of the half angle of the maximum cone of light that can exit from the optic, is increased, resulting in an increased resolution. The Abbe formula gives the smallest distance Δx (half pitch) which can be resolved by using radiation with a wavelength λ:

$$\Delta x = \frac{k_1 \lambda}{\mathrm{NA}} = \frac{k_1 \lambda}{n \sin \theta}. \quad (1)$$

Here, k_1 is a numeric constant from a Bessel function, λ is the vacuum wavelength. The numerical aperture is given by the opening angle θ, and the refractive index n of the medium. In this way, immersion fluids with refractive indices $n>1$ enable $\mathrm{NA}>1$. Currently, in immersion lithography water is used as the immersion fluid. In the imaging optics, the lenses are made of either fused silica, or calcium fluoride (CaF_2). The refractive index of fused silica at the operation wavelength is $n_{FS}=1.560\,22$, so not far from the one of calcium fluoride ($n_{CaF2}=1.50143$), and only slightly higher than the refractive index of water, which is 1.436. If one wants to further increase the resolution in microlithography by using fluids with higher refractivity, consequently, at least for the last imaging lens element, a material with an even higher refractive index is needed to avoid total reflection. Recently, oily fluids made of fluorinated polymers have been under development, providing refractive indices higher than 1.8. For the lens material, lutetium aluminum garnet (LuAG, $Lu_3Al_5O_{12}$) is the most promising material. It has a refractive index of about 2.14 at 193 nm, and has nearly isotropic optical properties due to its cubic structure. However, the electronic band gap of the LuAG crystal is close to the operation wavelength. This means that the transmission of LuAG at this wavelength is a critical parameter, since absorption in the band-gap region can be influenced by external parameters (e.g., crystal impurities) as well as intrinsic effects (e.g., exciton levels). Therefore, highly accurate measurements are needed to clearly show whether the transmission needed for lithographic imaging can be reached in principle with the chosen material. The scaling laws of the transmission in the vicinity of the band gap, the so-called Urbach (or Urbach-Martiensen) tails, provide a method to clearly identify an intrinsic absorption mechanism which will finally limit the transparency of the material.

This paper is structured as follows: In Sec. II, the measurements are described. Next, Sec. III explains how the relevant physical quantities are derived from the measured data. Section IV gives the physical description of the basic processes relevant for the interpretation of the data. Finally, the results are fitted in the context of the Urbach tail, and conclusions regarding the transmission properties of LuAG in the band-gap region are drawn.

II. EXPERIMENTS

To obtain the absorption data for LuAG, measurements were performed at the Physikalisch-Technische Bundesanstalt (PTB). Using monochromatized synchrotron radiation from PTB's metrology light source (MLS) low-energy electron storage ring,[1] the transmission and the reflection of LuAG samples with different sample thicknesses have been measured. The UV and vacuum ultraviolet (VUV) beamline

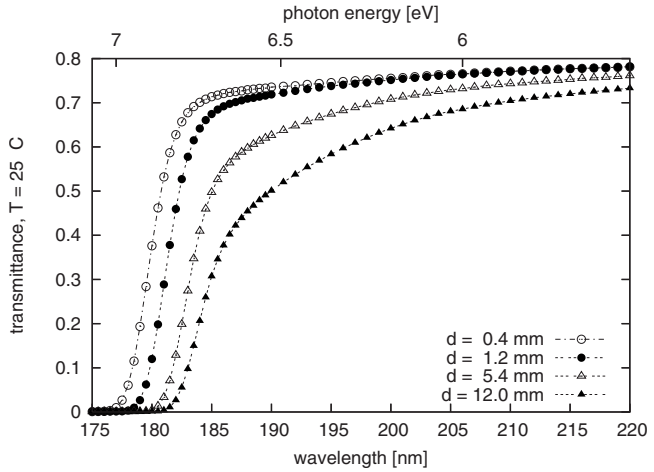

FIG. 1. Measured spectral transmittance of the four different LuAG samples with different thicknesses d at room temperature (25 °C) vs wavelength in the vicinity of the LuAG band gap.

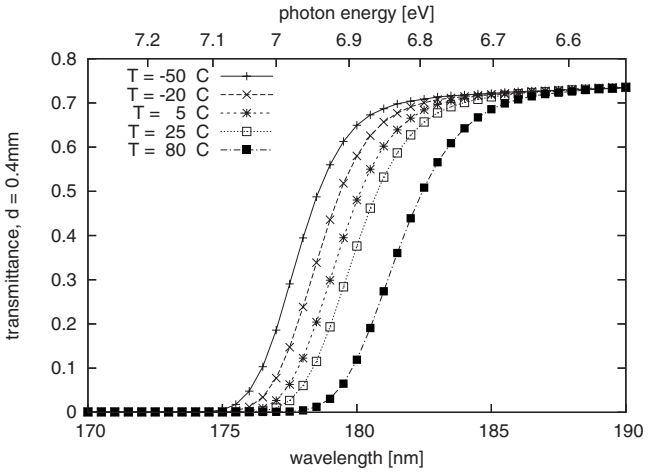

FIG. 2. Measured spectral transmittance of the LuAG sample with $d=0.4$ mm thickness plotted vs wavelength, with the temperature as a parameter, in the vicinity of the LuAG band gap.

for detector calibration and reflectometry provides tunable radiation from 40 to 400 nm with high-spectral purity, achieved in particular by the use of various bulk and gas filters for the suppression of higher grating orders from the monochromator. The spot size in focus amounts to 1 mm vertical by 2 mm horizontal at a spectral width of 1.7 nm at 193 nm. The typical radiant power for the measurements amounted to 1 μW. The wavelength is calibrated by the use of a spectral lamp and rare-gas absorption resonances with an overall wavelength uncertainty of 0.2 nm, and a reproducibility of 0.02 nm.

In an ultra-high-vacuum reflectometer, the transmission and reflectance of the samples were measured in a near-normal-incidence geometry. The incoming beam, as well as the transmitted or reflected beam, was measured by a semiconductor photodiode. This method allowed the absolute transmittance and reflectance to be measured with an uncertainty of typically a few 10^{-3}, depending of the sample surface quality and the wavelength-dependent spectral purity of the monochromatized radiation. Four samples of LuAG were provided from Schott Lithotec. The sample thicknesses were 0.4, 1.2, 5.4, and 12.0 mm (each with an uncertainty of 0.05 mm). The samples were cut from a single crystal grown at Schott Lithotec. The surface was polished in a multistep process with different diamond suspensions (down to 0.1 μm grain size) and finally treated with a chemical mechanical polishing (CMP) step. They were mounted into the reflectometer with a sample holder which allowed the samples to be set to variable temperatures, ranging from −50 °C (223 K) to 80 °C (353 K). For the measurements reported here, temperatures of −50 °C (223.15 K), −20 °C (253.15 K), +5 °C (278.15 K), +25 °C (298.15 K), and +80 °C (353.15 K) were chosen.

Figure 1 shows the result of the transmission measurements in the vicinity of the band gap, i.e., between 170 and 220 nm wavelength, for the four samples of different thicknesses at room temperature. In Fig. 2, we have plotted the measured transmittance vs wavelength for the different temperatures, for the thinnest sample with 0.4 mm thickness. On first sight, the transmission of each sample, not surprisingly, clearly depends on its thickness as well as on the temperature. However, the absorbance of the material cannot directly be determined from these measurements. To obtain the absorbance (or pure bulk transmittance), the reflected parts of the radiation have to be taken into account. Therefore, the spectral reflectivity was measured, too. Figure 3 shows the reflectivity for different temperatures, here for the thickest sample ($d=12$ mm). The reflectivity shows a strong dependence on the wavelength for wavelengths shorter than the band gap. The strong increase in reflectivity between 190 and 200 nm (6.0 and 6.7 eV, respectively) is due to the onset of transparency of the samples at the band gap. For longer wavelengths, the material is transparent and multiple reflections on both surfaces occur. For shorter wavelengths, the sample becomes nontransparent and all reflections from the second surface on the opposite side of the incoming beam

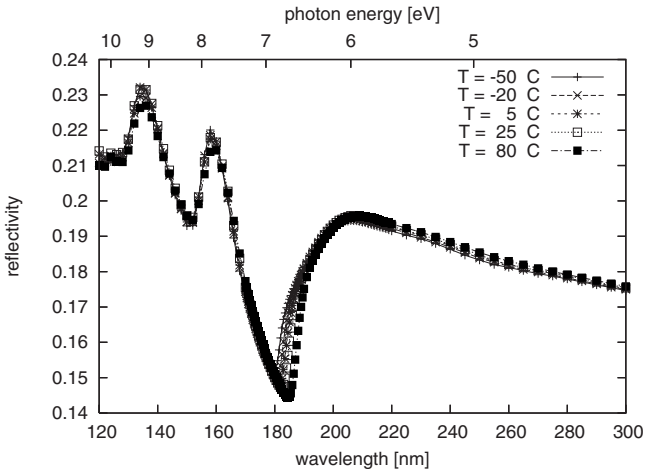

FIG. 3. Measured reflectance of the LuAG sample $d=12$ mm, with the temperature as a parameter. The strong increase in the reflectance between 190 and 200 nm (6 and 6.7 eV) is due to the onset of transparency of the material, and the resulting (multiple) reflections from the rear surface.

are lost. This effect has to be considered when interpreting the data to obtain the bare bulk transmittance of the material.

Additional and completely independent LuAG measurements were performed at MIT Lincoln Laboratory. For these measurements, four polished LuAG samples were received. The thicknesses of the four samples were 1, 3, 7, and 15 mm, respectively. Their optical properties were measured as received without any further surface cleaning. The transmission of all the samples was measured in a Hitachi U-4000 system (190 to 600 nm) and a Varian CARY DUV system (175 to 210 nm). The reflection of the thinnest sample was measured on an Acton CAMS VUV system from 170 to 300 nm. The reflection of the thicker samples could not be measured reliably as the rear surface reflection could not be fully captured into the reflectometer detector. However, as discussed in the data evaluation section, knowing reflection from just the thinnest sample is sufficient to extract accurate absorbance data for all the samples.

III. DATA EVALUATION

In the basic form, the bare bulk transmittance t for radiation of a wavelength λ passing through a material is given by the well-known Lambert-Beer law

$$t = e^{-\alpha d_i}, \tag{2}$$

where α is known as the extinction coefficient, and d_i the thickness of the sample. The absorbance A is commonly defined as $-\ln t$, however, in some cases it is common to take the log to the base 10. The extinction coefficient (and therefore the bulk absorbance) α is connected to the refractive index by

$$\alpha = \frac{4\pi\kappa}{\lambda}, \tag{3}$$

where κ is the (unitless) imaginary part of the refractive index of the medium (LuAG in our case), and λ is the wavelength. Together with the real part n of the refractive index, it defines the reflectivity of the material:

$$r = \left| \frac{n + i\kappa - 1}{n + i\kappa + 1} \right|^2. \tag{4}$$

In the general case, the measurement of the reflected and transmitted intensities (τ, R) does not directly give the reflectivity r and pure bulk transmittance t of the material, since (multiple) reflections from the sample rear surface have to be considered.

By calculating the (infinite) sum over all contributions and neglecting surface scattering and absorption, one obtains:

$$t(\tau,R) = \frac{-1-(R-2)R+\tau^2+\sqrt{4(R-2)R+(1-(R-2)R+\tau^2)^2}}{2\tau}, \tag{5}$$

$$r(\tau,R) = \frac{-1+(R-2)R-\tau^2+\sqrt{4(R-2)R+(1-(R-2)R+\tau^2)^2}}{2(R-2)}. \tag{6}$$

In Fig. 4, the reflectivity $r(\tau,R)$ as well as the measured reflectance R are depicted. For small photon energies, i.e., below the band gap where the material is still almost transparent, there is a strong difference between r and R due to the contributions from the multiple reflections passing through the sample. For larger photon energies, above the band gap of the material, the absorption is large enough for no multiple reflection to occur. We use the following definition for the terminology: The words "transmission" and "reflection" describe the process which happens to radiation, the "transmittance" and "reflectance" are the measured values of radiation intensity. As "absorptance" or "absorptivity" we understand the absorbed part of a radiation, which enters into Eq. (2) as an "absorption coefficient" or "absorbance" α.

Additionally, when determining the absorbance from the measurements, a surface contribution has to be taken into account, which originates from scattering at the surface, and therefore does not depend on the sample thickness. The existence of such a contribution becomes obvious if the extinction coefficient α, i.e., $-\log[t(\tau,R)]/d$, is plotted over the wavelengths for the four different samples (with different thicknesses d), as shown in Fig. 5: Since the extinction coefficient should be independent of the sample thickness, all curves should fall on the same master curve in the limit of longer wavelengths (lower photon energies), where the samples are transparent to the radiation. However, the differences especially at lower photon energies, clearly show that there is a non-negligible surface contribution to the extinction originating either from absorption or scattering. To account for this, we have modified Eq. (2) by a surface term s which is supposed to be identical for all four samples (indexed i),

$$t_i = e^{-(\alpha d_i + s)}. \tag{7}$$

To determine s, we have taken a pair of the measured samples,

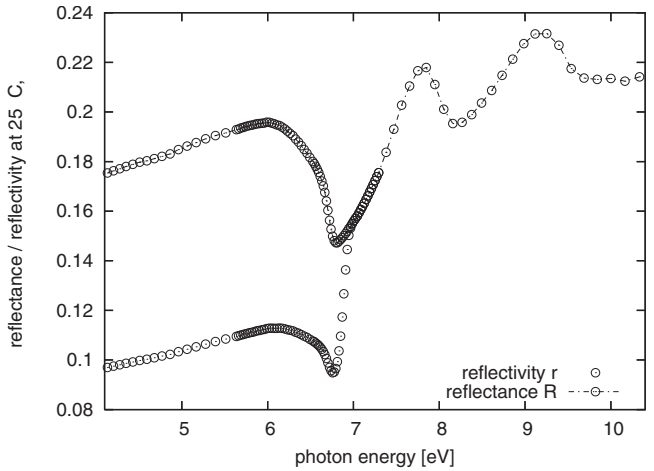

FIG. 4. The bare reflection $r(\tau,R)$(reflectivity), which accounts for multiple reflections, is plotted together with the (directly measured) reflectance R as a function of photon energy. For small photon energies there is a strong difference since the material is transparent and multiple reflections are important. For larger photon energies the material is in transparent, multiple reflection does not occur, and the two curves merge.

$$s = \frac{d_j \log t_i - d_i \log t_j}{d_j - d_i}, \tag{8}$$

where the indices i,j refer to two different samples of different thicknesses d_i and d_j. If the surface terms were exactly identical for all samples, we should observe for all six combinations of pairs (which we can choose from the four samples) six identical surface absorptions. Although this is not exactly the case, the result shown in Fig. 6 is still satisfying. For small photon energies, the surface term is nearly identical for all six combinations. Close to the band gap, the combination of the two thinnest samples is expected to give the best accuracy, since they should show the largest relative contributions from the surface term.

Because our interest is focused on the 193 nm wavelength, in Fig. 7 we have shown an alternative way to determine s for a single wavelength. Here, $\ln(t/t_0)$ is plotted as a function of sample thickness for the three thickest samples at 193 nm wavelength. Here t is the transmittance according to Eq. (5) and t_0 is the transmittance with only surface reflections due to the refractive index of a perfect surface. If the surface contribution is identical, all measurements then lay on a straight line with the y-axis zero point being the surface contribution, which in our case is determined to be 0.065.

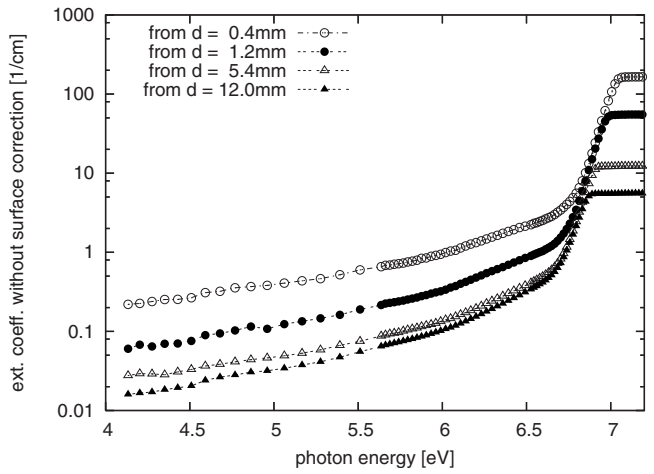

FIG. 5. Plot of the calculated absorption of LuAG (incl. surface contributions) vs. the photon energy in the band gap region.

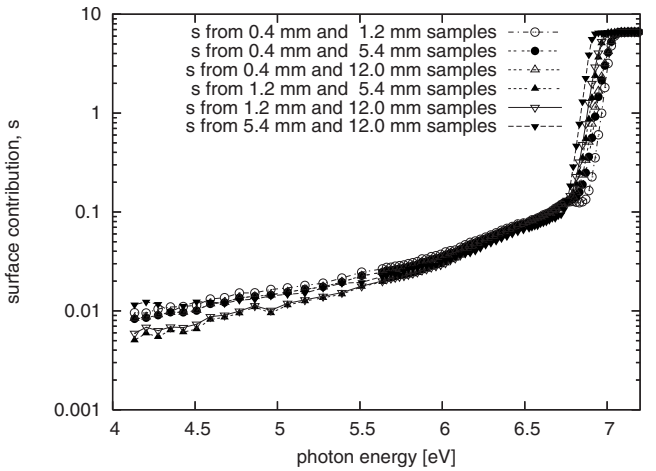

FIG. 6. The surface contribution s according to Eq. (8) plotted as a function of photon energy. The surface contribution obtained in this way is independent of the choice of the pair. This indicates a good and reliable surface polish.

In the same way we can combine pairs of samples to obtain the extinction coefficient α. Again, this should give the same result for any two combinations of thicknesses, if all the surfaces show identical absorption and scattering. In Fig. 8, we have plotted the absorbance from the six possible combinations for choosing pairs out of four samples. With the exception of the thinnest pair, the low-energy absorbance is in fair agreement for all different combinations. For larger photon energies around the band gap, the pair from the two

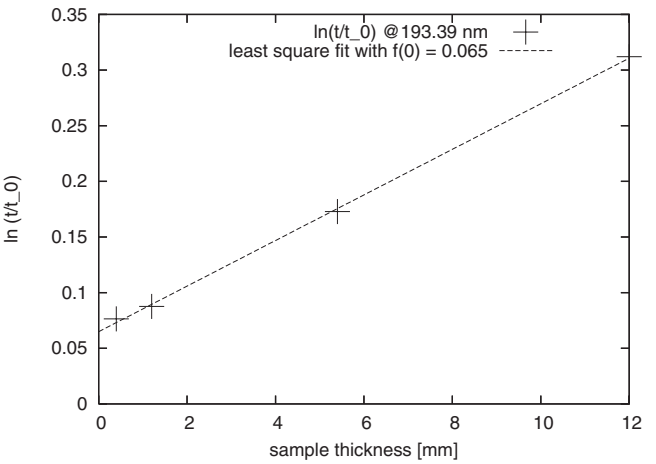

FIG. 7. The surface contribution for the wavelength of 193 nm can be extrapolated by plotting the quantity $\ln(t/t_0)$ as a function of sample thickness. The y-axis intercept is the (dimensionless) surface absorption. For 139.39 nm, this is in our case 0.065 (based on log e).

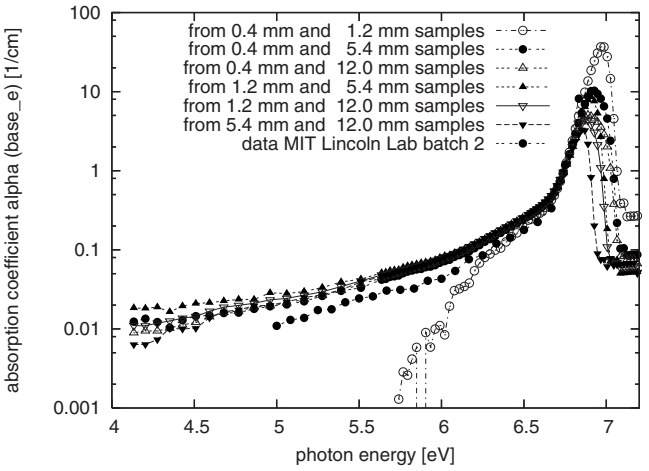

FIG. 8. For all six possible combinations of pairs out of four samples, we have plotted the resulting absorbance (base e). With the exception of the two thinnest samples the low-energy absorbance is quite independent on choosing the sample pair. For large photon energies around the band gap the pair from the two thinnest samples has the best accuracy. For comparison, the results of the absorbance measurements from the MIT Lincoln Laboratory are added.

thinnest samples gives the best results due to its better transparency. Therefore, we have fitted the steep part of the absorbance close to the band gap again from the two thinnest samples.

In Fig. 8, the results of completely independent measurements from the MIT Lincoln Laboratory are added for comparison.[2] As mentioned in the Experiments section, the MIT Lincoln Laboratory data included transmission measurements for four sample thicknesses and reflectance data for the thinnest sample (1 mm thick). For the 1 mm sample, we have modeled n and k optical constants of LuAG from the reflection/transmission data with a Kramers-Kronig-consistent dispersion relation, using a FILMWIZARD package from SciSoft corporation. The modeled refractive index dispersion data were forced to pass through the measured NIST value of 2.14 at 193 nm.[3] Once the optical constants of LuAG were obtained in this fashion, they were used to calculate expected reflection losses for all four LuAG samples, accounting for the double-sided reflection effects.

Finally, from the measured transmission and modeled reflection data, we obtained absorption data for every sample as a function of wavelength from 175 nm to 600 nm, neglecting scatter effects. To calculate absorbance per cm, at each wavelength we calculated the slope of absorption vs. thickness for the four samples.

IV. LOSS MECHANISMS CONTRIBUTING TO ABSORBANCE

The mechanisms were already discussed by some of us in a previous publication,[4] however, for a clearer understanding, the main points will be recapitulated here. It is known that in an ideal, perfect insulating single crystal, completely free of defects and at zero temperature, the first optical excitation is expected to occur at the photon energy where the radiation creates electron-hole pairs. In a strongly ionic system, such as many oxide and fluoride crystals, there is the possibility to excite into a two particle bound state of the electron and the hole: the exciton. Excitonic effects are discussed as important for YAG crystals in.[5] In LuAG, the lowest lying known absorption is at 7.8 eV and is probably caused by the Γ-exciton. The one-particle continuum (sometimes also called electron-hole continuum) starts at larger photon energies. We call this a one particle continuum since a photon excites one electron and creates an electron-hole pair which is in this case noninteracting. Electron and hole move independent from each other as single particles opposite to excitons. The different contributions to the absorbance can be described by different mechanisms leading to a loss of transmission.

A. Extrinsic loss due to disorder in the lattice

The most common type of defect in real crystals are impurity ions which are point defects leading to localized electronic impurity states very close to the band gap. In LuAG with a lattice constant of approx. 11.92 Å and 160 atoms in the elementary cell ($Lu_{24}Al_{40}O_{96}$), one ppb (parts per billion) of impurities already means that the average distance between neighboring impurities is $\sqrt[3]{10^6(1.2\ \text{nm})^3}=120$ nm, which is already much smaller than the wavelength of most applied radiations, but is, to give an order of magnitude, still of the order of the wavelength in material for deep ultraviolet (DUV) photolithography.

B. Intrinsic loss due to intrinsic defects

Even in an ideal crystal without any contamination by impurity atoms, defects occur due to the fact that crystal growth does not take place at zero absolute temperature but around the melting point of the crystal, which is 2010 °C (2283 K) for LuAG. Therefore, entropy will already introduce a number of intrinsic defects such as Lu antisites[6–8] and/or oxygen vacancies. These defects will lead to localized electronic states close to the band gap, too.

C. Intrinsic loss due to trapping of excitons in lattice distortions

A third mechanism is related to temporarily trapping excitons. In literature, this is described by two different models: Ihm and Phillips,[9] John *et al.*[10] as well as Schmitt-Rink *et al.*[11] mostly refer to the work of Toyozawa,[12,13] who describes a temporary trapping of excitons, and later Dow and Redfield in a series of articles,[14–16] who describe a model of field ionized excitons. Both models point out that the interaction between the exciton and other elementary excitations is the crucial point in understanding.

Normally, the photon energy has to be equivalent to the band gap in order to excite a free-electron-hole pair. In strongly ionic solids, where the screening of the Coulomb interaction by mobile charge carriers is not too strong, an excitonic electron-hole bound state can be formed at somewhat lower energies. In LuAG, the exciton exists probably around 7.8 eV, whereas the band gap is a little larger. Fol-

lowing the ideas of Toyozawa,[12] such electron-hole pairs can further lower the electronic energy, which is needed to excite them by interacting with a lattice distortion. The larger the temperature, the more lattice distortions are present. We can understand this phenomenon as electron-hole pairs, which virtually and temporarily jump into a lattice distortion and back. During the time when the electron-hole is in the lattice distortion, the photon energy needed for an excitation can be reduced, which leads to absorptions below the threshold of the bare exciton, i.e., below 7.8 eV for LuAG. This means that the exciton, which is usually delocalized and shows a particular dispersion, can be temporarily localized due to the interaction with (optical) phonon modes.

For insulators, there is a very universal scaling of the extinction coefficient around the band gap. This is called the Urbach or Urbach-Martiensen tail.[17,18] It has the general form

$$\alpha(\omega) = \alpha_0 e^{A(\hbar\omega - E_0)}, \tag{9}$$

where E_0 is the energy of the band gap at zero temperature, $\omega = 2\pi\nu = 2\pi c/\lambda$ is the angular frequency, $\hbar$ the Planck constant and α_0 and A are fit parameters. Since the number of available phonons is a function of temperature, the parameter A shows for ionic insulators at sufficiently large temperatures a well-defined temperature dependence

$$\alpha(\omega) = \beta_0 e^{(\sigma e(\hbar\omega - E_0)/k_B T)}, \tag{10}$$

where k_B is the Boltzmann constant, σ is a new fit parameter and e the electron charge. For common insulators[19] such as CuCl or TlCl, the parameter α_0 is of the order of 10^4 cm^{-1} and σ is of the order of 1. For CaF_2, recent results have been determined accordingly to the method described here.[4]

V. FIT OF THE URBACH-MARTIENSEN TAIL

In the following, we will discuss our results in the context of the Urbach tail, in particular concerning the absorption resulting from the intrinsic losses described in Sec. IV C. These would occur even in a perfect crystal, which is free of defects, hence limiting the transmission of any optical component made of LuAG. To determine this contribution, we performed a fit of the temperature-dependent steep part of the Urbach tail. In Fig. 9, we have plotted the result of the fitting procedure. This result can be read as follows: On the y axis, a given extinction coefficient (or respective absorbance) can be chosen, which might be, e.g., the material requirements of a lens manufacturer. The x axis is the photon energy of the operating radiation. In the context of ArF photolithography, one is interested in the photon energy of 6.41 eV (which corresponds to the respective wavelength of 193.39 nm). If the point where the required absorbance crosses this photon energy is at higher values than the fit line for the room temperature Urbach tail, the material can, in principle, reach the requirement by its intrinsic absorbance.

Due to the temperature dependence, the absorbance of the material can be lowered with the temperature: As seen in Fig. 9, the temperature-dependent part of the Urbach tail shifts to higher energies with lower temperatures. Therefore, cooling of the material (or the lens) is a possibility to broaden the

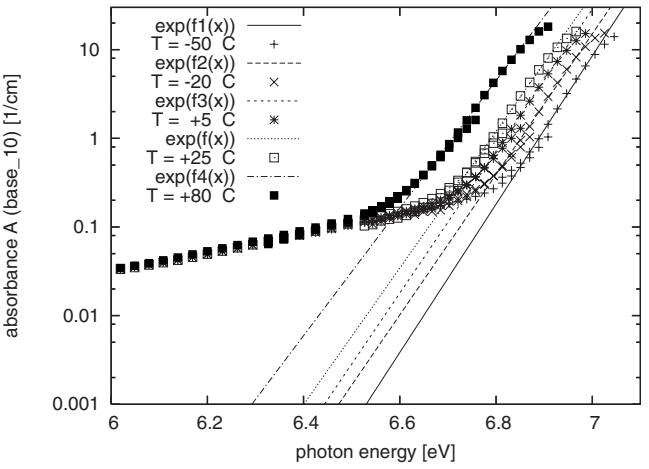

FIG. 9. Fit for the temperature-dependent contribution to the Urbach tail. On the y axis the absorbance A (based on $\log_{10}$) is plotted on a logarithmic scale. On the x axis the photon energy is plotted. The wavelength of 193.39 nm corresponds to 6.41 eV. Improvement in the crystal quality will only allow the temperature-independent part of the Urbach tail to be reduced. The temperature-dependent part is of intrinsic nature. The different fits for the temperature-dependent part of the Urbach tail we have labeled with exp[f1(x)], exp[f2(x)], exp[f3(x)], exp[f(x)], and exp[f4(x)] for the temperatures −50 °C, −20 °C, +5 °C, +25 °C, and +80 °C, respectively.

range of applicability of the material by an enlargement of the band gap. If we expand the absorbance at 193.39 nm for temperatures T around room temperature (RT=25 °C) we obtain:

$$\alpha(T,\omega) = a_{\mathrm{RT}} + w_1(T - \mathrm{RT}) + [b_{\mathrm{RT}} + w_2(T - \mathrm{RT})]\omega, \tag{11}$$

where $a_{\mathrm{RT}} = -120.472$ $[\mathrm{cm}^{-1}]$ and $b_{\mathrm{RT}} = 17.743$ $[\mathrm{eV}^{-1}\,\mathrm{cm}^{-1}]$ are the fit parameters for the fits in Fig. 9. $w_1 = 0.2603$ $[\mathrm{K}^{-1}\,\mathrm{cm}^{-1}]$ and $w_2 = -0.035$ $[\mathrm{eV}^{-1}\,\mathrm{K}^{-1}\,\mathrm{cm}^{-1}]$ are the expansion coefficients for the temperature dependence. This means the intrinsic absorbance is suppressed by $4.6 \cdot 10^{-5}$ $(\mathrm{cm\,K})^{-1}$, so that each degree of cooling reduces the intrinsic transmission by $4.6 \cdot 10^{-5}$ cm^{-1} at the wavelength of 193.39 nm. On the other hand, if a specification for an optical system demands a certain extinction coefficient, we can increase the intrinsic operation range of the band gap by 1.75 meV/K. This is already a strong increase and should be considered as a serious option.[20]

VI. CONCLUSION

The measurement of temperature-dependent Urbach tails clearly allows one to distinguish between the different parts of the Urbach tail. A temperature-dependent tail and a temperature-independent part, which mainly originates from intrinsic defects, are present. The latter can be suppressed by further improving the crystal growth and the purity of the raw materials. The second part, the temperature-dependent part of the Urbach tail, is of intrinsic nature and sets a clear limit for the transparency which can be reached. Above all,

we have derived the following conclusions: (i) For the wavelength of 193.39 nm (or 6.41 eV photon energy), the absorbance A (in terms of logarithm to the base 10) is limited as shown in Fig. 9 to a minimum of $A=1.18\cdot10^{-3}$. (ii) Cooling is an option to reduce the intrinsic absorbance[20] according to Eq. (11) by $4.6\cdot10^{-5}$ $(\mathrm{cm\ K})^{-1}$. (iii) There is a residual contribution hidden which is temperature independent, due to, e.g., antisites and which is difficult to remove. This contribution can be of the order of 10^{-3}. (iv) At the current surface polishing quality, the surface contribution to the absorption at 193.39 nm is $\ln(t/t_0)=0.065$ and has to be improved to meet the requirements. Currently, for a sample of at least 3 cm thickness, the intrinsic bulk absorption starts to exceed the current surface contribution. Growing a crystal, which is reasonably transparent at 193.39 nm and fabricating lens elements out of it remains a challenging goal and requires an impurity concentration at a single digit ppb level. However, this seems to be feasible if efforts are strengthened.

ACKNOWLEDGMENTS

The Lincoln Laboratory portion of this work was performed under a Cooperative Research and Development Agreement between MIT Lincoln Laboratory and SEMATECH.

[1] R. Klein, G. Brandt, R. Fliegauf, A. Hoehl, R. Müller, R. Thornagel, G. Ulm, M. Abo-Bakr, J. Feikes, M. v. Hartrott, K. Holldack, and G. Wüstefeld, Phys. Rev. ST Accel. Beams **11**, 110701 (2008).
[2] P. A. Zimmerman, B. J. Rice, E. C. Piscani, and V. Liberman, Proc. SPIE **7274**, 727420 (2009).
[3] J. H. Burnett, S. G. Kaplan, E. L. Shirley, D. Horowitz, W. Clauss, A. Grenville, and C. Van Peski, Proc. SPIE **6154**, 615418 (2006).
[4] M. Letz, A. Gottwald, M. Richter, and L. Parthier, Phys. Rev. B **79**, 195112 (2009).
[5] Y.-N. Xu, Yu Chen, S.-D. Mo, and W. Y. Ching, Phys. Rev. B **65**, 235105 (2002).
[6] V. Babin, M. Kink, Y. Maksimov, K. Nejezchleb, M. Nikl, and S. Zazubovich, J. Lumin. **122-123**, 332 (2007).
[7] V. Babin, K. Blazek, A. Krasnikov, K. Nejezchleb, M. Nikl, T. Savikhina, and S. Zazubovich, Phys. Status Solidi **2**, 97 (2005).
[8] Y. Zorenko, Phys. Status Solidi **2**, 375 (2005).
[9] J. Ihm and J. C. Phillips, Phys. Rev. B **27**, 7803 (1983).
[10] S. John, C. Soukoulis, M. H. Cohen, and E. N. Economou, Phys. Rev. Lett. **57**, 1777 (1986).
[11] S. Schmitt-Rink, H. Haug, and E. Mohler, Phys. Rev. B **24**, 6043 (1981).
[12] Y. Toyozawa, Prog. Theor. Phys. **20**, 53 (1958).
[13] Y. Toyozawa, Prog. Theor. Phys. **22**, 455 (1959).
[14] J. D. Dow and D. Redfield, Phys. Rev. B **1**, 3358 (1970).
[15] J. D. Dow and D. Redfield, Phys. Rev. Lett. **26**, 762 (1971).
[16] J. D. Dow and D. Redfield, Phys. Rev. B **5**, 594 (1972).
[17] F. Urbach, Phys. Rev. **92**, 1324 (1953).
[18] W. Martienssen, J. Phys. Chem. Solids **2**, 257 (1957).
[19] E. Mohler and B. Thomas, Phys. Rev. Lett. **44**, 543 (1980).
[20] M. Letz, L. Parthier, DE 10 2008 023238 A1 (2008).